Surface fluid registration and multivariate tensor-based morphometry in newborns - the effects of prematurity on the putamen

Jie Shi[1], Yalin Wang[1], Rafael Ceschin[2], Xing An[1], Marvin D. Nelson[3], Ashok Panigrahy[2], Natasha Leporé[3]
[1] Computer Science and Engineering, Arizona State University Tempe, AZ, USA
[2] Radiology, Childrens Hospital of Pittsburgh of UPMC, Pittsburgh, PA, USA
[3] Radiology, University of Southern California and Childrens Hospital, Los Angeles, CA, USA

***Abstract*— Many disorders that affect the brain can cause shape changes in subcortical structures, and these may provide biomarkers for disease detection and progression. Automatic tools are needed to accurately identify and characterize these alterations. In recent work, we developed a surface multivariate tensor-based morphometry analysis (mTBM) to detect morphological group differences in subcortical structures, and we applied this method to study HIV/AIDS, William's syndrome, Alzheimer's disease and prematurity. Here we will focus more specifically on mTBM in neonates, which, in its current form, starts with manually segmented subcortical structures from MRI images of a two subject groups, places a conformal grid on each of their surfaces, registers them to a template through a constrained harmonic mapping and provides statistical comparisons between the two groups, at each vertex of the template grid. We modify this pipeline in two ways: first by replacing the constrained harmonic mapping with a new fluid registration algorithm that we recently implemented. Secondly, by optimizing the pipeline to study the putamen in newborns.**

Our analysis is applied to the comparison of the putamen in premature and term born neonates. Recent whole-brain volumetric studies have detected differences in this structure in babies born preterm. Here we add to the literature on this topic by zooming in on this structure, and by generating the first surface-based maps of these changes. To do so, we use a dataset of manually segmented putamens from T1-weighted brain MR images from 17 preterm and 18 term-born neonates.

Statistical comparisons between the two groups are performed via four methods: univariate and multivariate tensor-based morphometry, the commonly used medial axis distance, and a combination of the last two statistics. We detect widespread statistically significant differences in morphology between the two groups that are consistent across statistics, but more extensive for multivariate measures.

I. Introduction

The putamen is affected in a number of disorders of the central nervous system and in particular, several recent MRI studies have shown morphological differences in this structure in neonates and adolescents born preterm. For example, a whole-brain deformation-based morphometry study [3] found significant reduction of lentiform nuclei in premature neonates compared to term-born controls. In addition, using voxel-based morphometry, [19] detected changes in the putamen in adolescents born very prematurely.

These studies highlight the need for a more detailed assessment of this structure in premature children. However, none of the morphometric studies in these subjects to date has zoomed in specifically on the putamen. In addition, all studies so far have been volumetric studies, but as shown in several previous studies (see e.g. [34], [33]) important complementary information may be found through surface-based analyses. Putamen lesions have been implicated in impaired visual function in newborn [16]. Given the involvement in the putamen in disorders such as cerebral palsy that can affect premature children, and it's role in various forms of learning, a more detailed assessment of the effect of prematurity on this structure is sorely needed.

The contributions of this work are 3-fold. First, we propose a novel pipeline for group comparisons of the surface anatomy of the putamen in neonates that involves conformal grid generation, fluid registration and a multivariate tensor-based morphometry (mTBM) statistical analysis. Fig. 1 illustrates our pipeline. Surface mTBM has been applied to the ventricles, the thalamus, the hippocampus and the corpus callosum of premature neonates [34], [22], [36], [37]. In these studies and those of subcortical structures in adults (e.g. [32]), mTBM increased statistical power to detect statistical differences between groups, and improved the localization of the changes. We expect similar results with the methods described here.

Secondly, we validate a new fluid registration algorithm, for which we extend the Navier-Stokes equation into general surface space using covariant derivatives [22]. Due to the simple Riemannian metric induced by conformal parameterization, this general Navier-Stokes equation is easy to compute and is adjusted for the area distortion. Compared with early works such as [27], our formulation is much simpler and provides more accurate registration results.

Finally, we perform the first ever group analysis of the surface of the putamen in premature neonates. More specifically, starting from a data set of T1-weighted brain MRI, we compare the manually segmented putamens of 17 preterm and 18 term-born newborn subjects using a pipeline that we recently implemented for the surface analysis of subcortical structures in neonates (see [34], [22]). We aim to detect surface-based regional differences in shape between the two groups. Our method involves conformal grid generation on the surface [30], surface fluid registration [22] and a multivariate tensor-based morphometry statistical analysis [32]; it has been shown to

increase detection power in our neonatal studies [34], [37], and in adults [32]. We focus exclusively on preterm neonates with no visible evidence of white matter injury as determined by an expert neuroradiologists, in order to determine whether subtle brain injuries are still present in those subjects, and whether our pipeline is sensitive enough to detect smaller changes. Our work provides the first precise subparcellation of the putamen in premature neonates and allows for more regional specificity than previous group analyses in these subjects.

II. Method

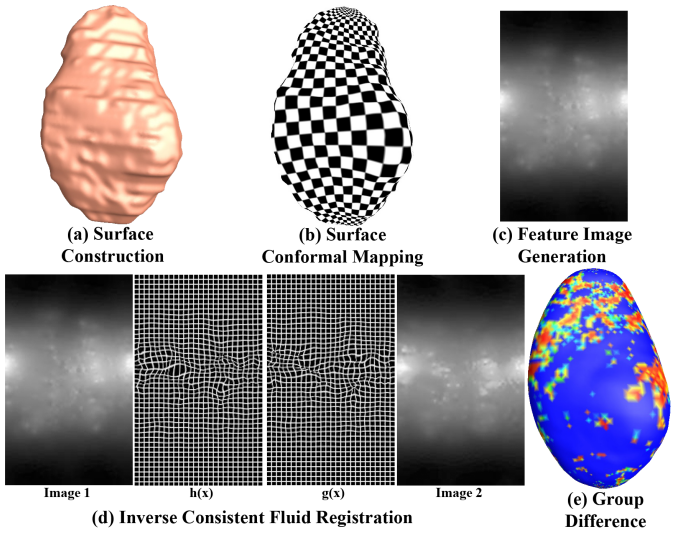

Fig. 1. The proposed system. The putamen is segmented from T1-weighted images (a). A conformal grid is built on the surface (b), and fluidly registered to a common template (c,d). Surface mTBM is applied to analyze morphometric changes (e)

A. Neonatal Data

Our dataset comprises 17 premature neonates (gestational ages 25-36 weeks, 43.02 $\pm$ 1.7218 weeks at scan time) with normal MR scans and 18 healthy term born infants (gestational ages 43.0150 $\pm$ 1.7392 weeks at scan time).

T1-weighted MRI scans were acquired using a dedicated neonatal head coil on a 1.5T GE scanner using a coronal three-dimensional spoiled gradient echo sequence. The inclusion criteria for our preterm subjects were the following: 1) prematurity, and 2) visually normal scans on conventional MRI. Structural MRI are qualitatively classified as controls by 2 board certified neonatal neuroradiologists. The institutional review board at our medical center approved the study protocol.

Term neonates with diffusion weighted abnormalities, elevated lactate as determined by MR spectroscopy, chromosomal/mitochondrial diseases, ECMO, hypotonia at birth and other syndromes with poor neurological outcomes were excluded. Preterms were excluded based on chromosomal diseases or major neurological exam abnormalities, or if they exhibited brain lesions including: (1) focal white matter necrosis as definite as cavitary/non-cavitary lesions (2) diffuse ventriculomegaly (3) significantly increased subarachnoid space and sulcal enlargement (4) diffuse excessive T2 hyperintensity by visual criteria. Clinical information such as premature rupture of membranes, apgar scores, postnatal sepsis, ventilation and retinopathy of prematurity are retrospectively reviewed from the NICU database for the for determination of other clinical risk factors.

We manually segment the putamen with Insight Toolkit's SNAP program [39]. Tracings are done in the registered template space by an experienced pediatric neuroradiologist, using standard protocols. Fig. 1 shows an example of a reconstructed surface and its surface mesh for one subject.

B. Surface Grid Generation

We compute conformal grids on each of the segmented putamens using a method based on holomorphic differentials, as described in [30]. The resulting surface parameterizations are very robust and stable, and our grid computation method is intrinsic and efficient because the conformal grid computation is done by solving a linear system of equations [30].

One challenge to generate parametric surfaces for subcortical structures is the complicated topology, e.g. long and thin tail in caudate and multiple-arm structure of the lateral ventricles. A canonical space such as a sphere [25] typically generates a lot of distortion in these cases [32]. On the other hand, conformal geometry may conformally map topologically complex surfaces to a plane. The key step to turning this nonlinear conformal parameterization problem into a linear one is to have a topology optimization step [30]. For example, here we leave 2 holes and model the putamens as surfaces that are topologically equivalent to a cylinder with two open boundaries. By computing a special group of holomorphic 1-forms, we achieve consistent conformal parameterization. By tracing equal parameter coordinates, we conformally map the putamen surface to a complex domain.

We have successfully applied this method in adults to process hippocampal and lateral ventricular surfaces in HIV/AIDS and Alzheimer's disease studies [32], [33], and in neonates in the ventricules, hippocampus and thalamus and corpus callosum [34], [37], [36]. The induced parametrization is one-to-one, angle-preserving, and preserve small similarities between surfaces. An example of the grids that we generated is shown in Fig. 1.

C. Surface Fluid Registration

After computing surface geometric features, we align surfaces in the parameter domain with a fluid registration to maintain smooth, one-to-one topology [6], [4]. To simulate fluid flow on the surfaces, the Navier-Stokes equation is extended into surface space using the manifold version of Laplacian and divergence [1], [24]. .

Using harmonic mapping, we essentially convert the surface registration problem to an image registration one. In our prior work [29], we proposed an automated surface fluid registration method combining conformal mapping and image fluid registration [8] with mutual information [12], [17], [38], [21], [10] as the driving force of the viscous fluid. In [29], the

mutual information between two surface feature images, i.e., the conformal representations of the two surfaces that need to be registered, was maximized by the viscous fluid flow as in [8]. On R^2, fluid flow is governed by the Navier-Stokes equation. For compressible fluid flow, we have

$$\mu\Delta v(x) + (\mu + \tau)\nabla(\nabla.v(x) = f(x, u(x)). \quad (1)$$

Here $v(x)$ is the deformation velocity, and μ and τ are the viscosity constants. $f(x, u(x))$ is the force field that is used to drive the fluid flow, which was defined as the mutual information in [29]. To simulate fluid flow on Riemann surfaces, we need extend this equation into surface space by the manifold version of Laplacian and divergence [1], [24], [15]. By covariant derivatives, the Navier-Stokes equation for Riemann surface can be defined as [22]:

$$\frac{\mu}{\lambda}\Delta v + \frac{\mu + \tau}{\lambda}\nabla(\nabla.v) = f \quad (2)$$

where λ is the conformal factor. By the scaling factor λ, the Navier-Stokes equation is adjusted for the area distortion introduced by the conformal parameterization. As a result, Eq. 2 is now governing fluid flow on the manifolds. In this paper, considering that putamens across the population should have similar shapes, we assume the conformal representations of different putamens have similar intensity range and distribution. Thus, the body force f driving the fluid flow in this paper is defined as the sum of squared intensity differences (SSD) between the deforming image and the template image. In our experiments, the SSD based energy formulation has similar performance with mutual information energy which was adopted in our prior work [29] while significantly improves algorithm efficiency compared with the latter method. Since conformal mapping and fluid registration generate diffeomorphic mappings, a diffeomorphic surface-to-surface mapping is then recovered that matches surfaces in 3D.

As pointed out in [13], image registration problem should be symmetric, i.e., the correspondences established between the two images should not depend on the order we use to compare them. [13] proposed a novel inverse consistent image registration method. Instead of enforcing inverse consistency using an additional penalty that penalizes inconsistency error as in [7], the method in [13] directly modeled the reverse mapping by inverting the forward mapping. [5] replaced the linear elastic regularizer in [13] with the fluid regularization to enable large deformations and applied the inverse consistent fluid registration algorithm to diffusion tensor images. With the inverse consistent scheme proposed in [5], Eq. 2 can be extended into an inverse consistent surface fluid registration method. Let $I_1(x), I_2(x)$ be two images, using the sum of squared intensity differences as the matching cost function, the inverse consistent image registration problem seeks two mappings $h(x)$ and $g(x)$ to minimize the following energy function:

$$E(I_1(x), I_2(x)) = \int_\Omega |I_1(h(x)) - I_2(x)|^2 dx + \alpha R(h(x)) + \int_\Omega |I_2(g(x)) - I_1(x)|^2 dx + \alpha R(g(x)) \quad (3)$$

where $h(x) = x - u_f(x)$ is the mapping from image I_1 to image I_2 (forward direction) and $u_f(x)$ is the forward displacement field. $g(x) = x - u_b(x)$ is the mapping from image I_2 to image I_1 (backward direction) and $u_b(x)$ is the backward displacement field, $g(x) = h^{-1}(x)$. α is a positive scalar weighting of the regularization terms applied to the forward and backward mappings. Here we let $\alpha = 1$. Eq. 3 is symmetric and does not depend on the order of I_1 and I_2, i.e., $E(I_1, I_2) = E(I_2, I_1)$. With fluid regularization scheme, $R(h(x))$ is defined as $\int_0^1 \int_\Omega ||Lv_f(x)||^2 dxdt$ and $R(g(x))$ is defined as $\int_0^1 \int_\Omega ||Lv_b(x)||^2 dxdt$ with the forward and backward velocities $v_f(x)$ and $v_b(x)$, respectively. $L = \frac{\mu}{\lambda}\Delta + \frac{\mu+\tau}{\lambda}\nabla(\nabla.)$ is the surface linear operator as in Eq. 2. Then the energy function in Eq. 3 can be minimized by solving for the velocities $v_f(x)$ and $v_b(x)$ in the following general Navier-Stokes equations:

$$\frac{\mu}{\lambda}\Delta v_{f,b} + \frac{\mu + \tau}{\lambda}\nabla(\nabla.v_{f,b}) = f_{f,b} \quad (4)$$

where the forward force field $f_f = -[I_1(x - u_f(x)) - I_2(x)]\nabla I_1(x - u_f(x))$ and backward force field $f_b = -[I_2(x - u_b(x)) - I_1(x)]\nabla I_2(x - u_b(x))$. With the mappings $h(x)$, $g(x)$ initialized as the identical mapping at $t = 0$, the forward and backward mappings at time t are given by the following equations as in [13]:

$$h_t(x) = h_{t-1}(x) + \epsilon\eta_1(x) + \epsilon\eta_2(x) \quad (5)$$

$$g_t(x) = g_{t-1}(x) + \epsilon\xi_1(x) + \epsilon\xi_2(x) \quad (6)$$

Here, ϵ is an infinitesimally small positive time step. $\eta_1, \eta_2, \xi_1, \xi_2$ are computed as [5]:

$$\eta_1(x) = -(\nabla h_{t-1}(x))v_f^{t-1}(x), \eta_2(x) = v_b^{t-1}(h_{t-1}(x))$$
$$\xi_1(x) = v_f^{t-1}(g_{t-1}(x)), \xi_2(x) = -(\nabla g_{t-1}(x))v_b^{t-1}(x) \quad (7)$$

We map the surfaces grids to a common template (one of the controls), chosen at random. Since both the harmonic mapping and fluid registration generate diffeomorphic mappings, a diffeomorphic surface-to-surface mapping matches our surfaces in 3D.

D. Surface Registration by constrained harmonic mapping

We compare the fluid registration to a parametric surface approach to register the putamens that was implemented in [29]. The induced parameterization computes a one-to-one mapping from an anatomical surface to a plane, which serves as a canonical space to compute correspondences between surfaces [9], [26]. We register putamens surfaces across subjects using constrained harmonic maps. This approach is independent of the template mesh selection. The constrained harmonic map can be computed as follows.

Given two surfaces S_1 and S_2, whose conformal parameterizations are $\tau_1 : S_1 \rightarrow \Re^2$ and $\tau_2 : S_2 \rightarrow \Re^2$., we want to to find a map $\phi : S_1 \rightarrow S_2$. Instead of directly computing ϕ, we can find a harmonic map between the parameter domains. We look for a harmonic map, $\tau : \Re^2 \rightarrow \Re^2$, such that its composition with the conformal parametrization on S_1 gives the conformal parametrization on S_2:

$$\tau \circ \tau_1(S_1) = \tau_2(S_2), \tau \circ \tau_1(\partial S_1) = \tau_2(\partial S_2), \Delta\tau = 0,$$

where Δ is the Laplacian. Then the map ϕ may be obtained by $\phi = \tau_1 \circ \tau \circ \tau_2^{-1}$. Since τ is a harmonic map, and τ_1 and τ_2 are conformal maps, the resulting ϕ is a harmonic map.

E. Surface Multivariate Tensor-based Morphometry

Our ultimate aim is to determine the intrinsic surface morphology of segmented putamens in preterm neonates. We do so by applying a multivariate tensor-based morphometry analysis [14], [32], [33].

In tensor-based morphometry, for each subject in the data set, the registration yields a displacement field $\vec{u}$ between the template and the subject's images. A Jacobian matrix $J = Id + \nabla\vec{u}$ is computed at each vertex from the registration between template and subjects images, where Id is the identity matrix. These Jacobian matrices, or a function of their components are used as metrics for group comparisons. For example, the determinant, $detJ$ expresses the ratio of the surface area between the moving and fixed images while in mutlivariate tensor-based morphometry, we use the deformation tensors $S = \sqrt{(J^T J)}$ (in fact their logarithm [2], [14], [32]). S can be represented as a 2D ellipse at the center of each grid cell, whose axes show the direction and size of the change in area between the two surfaces at that location. In general, the multivariate measures yield increased statistical power when compared to the univariate ones (see e.g. [14] for the volume-based multivariate tensor-based morphometry and [32], [34] for the surface-based one).

In practice, the computation of the matrices are done using difference between edge lengths on the grid. Suppose $\phi : S_1 \rightarrow S_2$ is a map from surface S_1 to surface S_2. The derivative map of ϕ is the linear map between the tangent spaces $d\phi : TM(p) \rightarrow TM(\phi(p))$, induced by the map ϕ, which also defines the Jacobian matrix of ϕ. In the triangle mesh surface, the derivative map $d\phi$ is approximated by the linear map from one face $[v_1, v_2, v_3]$ to another $[w_1, w_2, w_3]$. First, the surfaces $[v_1, v_2, v_3]$ and $[w_1, w_2, w_3]$ are isometrically embedded onto the plane R^2, the planar coordinates of the vertices v_i, w_i are denoted by the same symbol v_i, w_i. Then the Jacobian matrix for the derivative map $d\phi$ can be explicitly computed as in [31]

$$J = d\phi = [w_3 - w_1, w_2 - w_1][v_3 - v_1, v_2 - v_1]^{-1}. \quad (8)$$

F. Medial Axis Method

One of the most commonly used morphometry measure on surface data is the radial distance ρ from a medial axis to a vertex of the surface [20], [27]. Here the medial axis is computed using the center point of the iso-parametric curves, on the conformal grid [33]. We will use the medial axis method as a complementary measure to the surface shape analysis from multivariate tensor-based morphometry.

G. Multivariate Statistical Analysis

We use a total of four different statistics: the deformation tensors S, the radial distance ρ, the determinant of the Jacobian matrix $detJ$ and a vector (S, ρ) containing the elements of S and ρ.

Since the S are positive definite matrices, they do not form a vector space under the usual matrix addition and scalar multiplication, so we can not use standard Euclidean statistics. Instead, they are transported to the tangent plane at the origin of the manifold of deformation tensors [2], where standard flat space statistics can then be used. In practice, all that this means is that mTBM statistics are computed on the matrix logarithm $\log(S)$ instead of directly on S.

For ρ and $detJ$, a standard voxel-wise t-test is used to compare the preterm to the term-born neonates, while for either of the multivariate tests on S or (S, ρ), group statistics are computed using the Hotelling's T^2 test [11] - the multivariate extension of the Student's t-test -, as described in [14], [32], [33]. In order not to assume a normal distribution, we run a vertex-based permutation test on the results [18], [14], [32]. We randomly assign diagnostic labels (premature or term-born) to each subject, without replacement. A t- or T^2-test is performed at each vertex using the new labels. The procedure is repeated 10000 times. We obtain a null distribution of t or T^2-values at each vertex to which we compare the t- or T^2-values from the real data.

III. Results

Figure 2 shows the surface statistics for all four statistics. Clusters of significance are found bilaterally, particularly on the anterior and inferior surface of the putamen. All measures give similar clusters of significance, though the multivariate measures are more powerful (but noisier) than the univariate ones, and only the combined statistics (S, ρ) reached significance. Clusters are primarily found in the anterior ventral part of the putamen, bilaterally.

Figure 3 shows a comparison of the fluid registration method compared to the constrained harmonic one. The two methods give similar clusters of significance, which provides a validation of the fluid registration method. The fluid registration results are noiser for surface-based statistics, though not for the radial ones, but they give results that are more powerful.

IV. Discussion

We applied a novel pipeline for surface based analysis of subcortical structures of neonates to compare the putamen in premature neonates compared to term born controls. We detected widespread areas of significance throughout the putamen. While all measures gave consistent results, the combined (S, ρ) statistic outperformed S all the other ones and is the only one to reach statistical significance when correction for

multiple comparisons are applied. It is interesting to note in particular that both ρ and S gave similar clusters of significance, though the later describes changes constrained to the surface, while the former gives radial information. In addition, we compared the fluid registration to the constrained harmonic map, and the former outperformed the later in terms of statistical significance.

The two registration methods are similar in nature as both of the convert surface registration problem to a familiar 2D image registration one via conformal parametrization. In comparison, the harmonic one relies more on geometry. On a convex polygon, the harmonic map is diffeomorphism. The limitation here is that it strongly depends on boundary conditions as we solve a Dirichlet condition to compute the harmonic map. The surface fluid registration method improves the registration by considering the important shape or functional features as image features for registration, so that it reduces the dependence on the boundary conditions. Fluid registration also allows large diffeomorphisms. However, its results are not very tight connection to surface intrinsic geometric features as we model shape features as explicit constraints.

The results found in the ventral-anterior portion of the putamen suggest that cortical-striatal-cortical thalamic connections are abnormal, particularly since the anterior putamen is interconnected to the limbic system [28]. However, more work is needed to confirm this hypothesis. One interesting surface putamen study [23] shows surface abnormalities in the ventral or anterior putamen in teenagers with attention deficit disorders (ADHD), similar to the results found here. As preterm neonates are at risk of developing ADHD, it would be of interest to understand the relationship with the results found here to the chances of developing ADHD later in life.

We are currently working on increasing the sample size to confirm the above results. In larger studies in adults, multivariate tensor-based morphometry outperformed univariate methods to detect brain differences in lateral ventricles in HIV/AIDS patients [32], and in a large Alzheimer's morphometry study (804 subjects) of subcortical structures [33]. We expect that this will be the case in neonates too.

In the future, we aim to correlate the above results with clinical outcome, and we will also perform group comparisons of the putamen between older premature and control children to see if the differences found here disappear with age.

The methods described here could be used for early detection and/or risk stratification of neurological problems and learning deficits so that innovative therapies and/or early intervention could be administered. In the immediate neonatal period, they could also be used to determine the effect of certain therapies (i.e. antibiotics, hypothermia, and/or pharmacologic agents) on the development of the putamen.

We have applied the methods here to preterm neonates, but they can be applied to study group differences in this structure from different neurological conditions in subjects of all ages. The pipeline may be downloaded freely at [35].

REFERENCES

[1] Aris R, Vectors, tensors, and the basic equations of fluid mechanics, Dover, 1989

[2] Arsigny V, Fillard P, Pennec X, Ayache N. Log-Euclidean metrics for fast and simple calculus on diffusion tensors. Magn Reson Med 56 (2):411-421, 2006

[3] Boardman JP, Counsell SJ, Rueckert D, Kapellou O, Bhatia KK, Aljabar P, Hajnal J, Allsop JM, Rutherford MA, Edward AD, Abnormal deep grey matter development following preterm birth detected using deformation-based morphometry. NeuroImage 32(1):70-78, 2006

[4] Bro-Nielsen M, Gramkow C. Fast fluid registration of medical images, Proceedings of the 4th International Conference on Visualization in Biomedical Computing, Hamburg, Germany. September 22-25:267–276, 1996

[5] Chiang MC, Leow AD, Klunder AD, Dutton RA, Barysheva M, Rose SE, McMahon KL, de Zubicaray GI, Toga AW, Thompson PM. Fluid registration of diffusion tensor images using information theory. IEEE Trans Med Imaging 27:442-456, 2008

[6] Christensen GE, Rabbitt RD, Miller MI. Deformable templates using large deformation kinematics, IEEE Trans. Image Process. 5:1435-1447, 1996

[7] Christensen GE, Johnson HJ. Consistent image registration. IEEE Trans Med Imaging 20:568-582, 2001

[8] D'Agostino E, Maes F, Vandermeulen D, Suetens P. A viscous fluid model for multimodal non-rigid image registration using mutual information. Med Image Anal 7:565-575, 2003

[9] Fischl B, Sereno MI, Dale AM. Cortical Surface-Based Analysis II: Inflation, Flattening, and a Surface-Based Coordinate System. Neuroimage 9:195-207, 1999

[10] Hermosillo G. Variational methods for multimodal image matching. PhD thesis, Université de Nice (INRIA-ROBOTVIS), Sophia Antipolis, France. 2002

[11] Hotelling H. The generalization of Student's ratio. Ann Math Statist 2:360-378, 1931

[12] Kim B, Boes JL, Frey KA, Meyer CR. Mutual information for automated unwarping of rat brain autoradiographs. Neuroimage 5:31-40, 1997

[13] Leow A, Huang SC, Geng A, Becker J, Davis S, Toga A, Thompson P. Inverse consistent mapping in 3D deformable image registration: its construction and statistical properties. Inf Process Med Imaging 19:493-503, 2005

[14] Lepore N, Brun C, Chou YY, Chiang MC, Dutton RA, Hayashi KM, Luders E, Lopez OL, Aizenstein HJ, Toga AW, Becker JT, Thompson PM. Generalized tensor-based morphometry of HIV/AIDS using multivariate statistics on deformation tensors. IEEE Trans Med Imag 27 (1):129-141, 2008

[15] Lui LM, Wang Y, Chan TF. Solving PDEs on Manifolds with Global Conformal Parametriazation. Variational, Geometric, and Level Set Methods in Computer Vision:307-319, 2005

[16] Mercuri E, Atkinson J, Braddick O, Anker S, Cowan F, Rutherford M, Pennock J, Dubowitz L. Basal ganglia damage and impaired visual function in the newborn infant. Archives of Disease in Childhood 77:F111F114 1997

[17] Meyer CR, Boes JL, Kim B, Bland PH, Zasadny KR, Kison PV, Koral K, Frey KA, Wahl RL. Demonstration of accuracy and clinical versatility of mutual information for automatic multimodality image fusion using affine and thin-plate spline warped geometric deformations. Med Image Anal 1:195-206, 1997

[18] Nichols TE, Holmes AP. Non parametric permutation tests for functional neuroimaging: a primer with examples. Hum Brain Mapp 25 (1):1-25, 2009

[19] Nosarti C, Giouroukou E, Healy E, Rifkin L, Walshe M, Reichenberg A, Chitnis X, Williams SCR, Murray RM. Grey and white matter distribution in very preterm adolescents mediates neurodevelopmental outcome. Brain 131:205-217, 2008

[20] Pizer S, Fritsch D, Yushkevich P, Johnson V, Chaney E. Segmentation, registration, and measurement of shape variation via image object shape. IEEE Trans Med Imag 18 (10):851-865, 1999

[21] Rueckert D, Sonoda LI, Hayes C, Hill DL, Leach MO, Hawkes DJ. Nonrigid registration using free-form deformations: application to breast MR images. IEEE Trans Med Imaging 18:712-721, 1999

[22] Shi J, Thompson PM, Gutman B, Wang Y, Surface Fluid Registration of Conformal Representation: Application to Detect Disease Burden and Genetic Influence on the Hippocampus, NeuroImage, submitted, 2012

[23] Sobel LJ, Bansal R, Maia TV, Sanchez J, Mazzone L, Durkin K, Liu J, Hao X, Ivanov I, Miller A, Greenhill LL, Peterson BS, Basal Ganglia Surface Morphology and the Effects of Stimulant Medications in Youth With Attention Deficit Hyperactivity Disorder, Am J Psychiatry 167:977986, 2010

[24] Stam J. Flows on Surfaces of Arbitrary Topology. Proceedings of SIGGRAPH, 724-731, 2003

[25] Styner M, Lieberman JA, McClure RK, Weinberger DR, Jones DW, Gerig G. Morphometric analysis of lateral ventricles in schizophrenia and healthy controls regarding genetic and disease-specific factors. Proc. Natl. Acad. Sci. U. S. A. 102(13):4872-4877, 2005

[26] Thompson PM, Giedd JN, Woods RP, MacDonald D, Evans AC, Toga AW. Growth Patterns in the Developing Human Brain Detected Using Continuum-Mechanical Tensor Mapping. Nature 404:190-193, 2000

[27] Thompson PM, Hayashi KM, de Zubicaray GI, Janke AL, Rose SE, Semple J, Hong MS, Herman D, Gravano D, Doddrell DM, Toga AW. Mapping hippocampal and ventricular change in Alzheimer's disease. NeuroImage 22:1754-1766, 2004

[28] Voorn P, Vanderschuren LJMJ, Groenewegen HJ, Robbins TW, Pennartz CMA. Putting a spin on the dorsalventral divide of the striatum, Trends in Neurosciences 27(8):468-474 (2004)

[29] Wang Y, Chiang MC, Thompson PM. Mutual Information-based 3D Surface Matching with Applications to Face Recognition and Brain Mapping. Proceedings ICCV, 527-534, 2005

[30] Wang Y, Lui LM, Gu X, Hayashi KM, Chan TF, Toga AW, Thompson PM, Yau ST. Brain surface conformal parameterization using Riemann surface structure. IEEE Trans Med Imag 26(6):853-865, 2007

[31] Wang Y, Dai W, Gu X, Chan TF, Yau ST, Toga AW, et al. Teichmller Shape Space Theory and Its Application to Brain Morphometry, Proceedings MICCAI , 133-140, 2009

[32] Wang Y, Zhang J, Gutman B, Chan TF, Becker JT, Aizenstein HJ, Lopez OL, Tamburo RJ, Toga AW, Thompson PM. Multivariate Tensor-based Morphometry on Surfaces: Application to Mapping Ventricular Abnormalities in HIV/AIDS. NeuroImage 49, 2141-2157, 2010

[33] Wang Y, Song Y, Rajagopalan P, An T, Liu K, Chou YY, Gutman B, Toga AW, Thompson PM. Surface-based TBM boosts power to detect disease effects on the brain: An N=804 ADNI study. Neuroimage 56(4):1993-2010, 2011b

[34] Wang Y, Panigrahy A, Shi J, Ceschin R, Nelson MD, Gutman B, Thompson PM, Lepore N. Surface Multivariate Tensor-based Morphometry on Premature Neonates: A Pilot Study. MICCAI workshop on Image Analysis of Human Brain Development, Toronto, Canada, September 22, 2011c

[35] Wang, Y., http://gsl.lab.asu.edu/conformal.htm, 2011a

[36] Wang Y, Panigrahy A, Shi J, Ceschin R, Nie Z, Nelson MD, Lepore N. 3D vs. 2D Surface Shape Analysis of the Corpus Callosum in Premature Neonates. MICCAI Workshop on Perinatal and Paediatric Imaging, Nice, France, Oct 1, 2012

[37] Wang Y, Panigrahy A, Shi J, Ceschin R, Nelson MD, Gutsman B, Thompson PM, Lepore N. Ventricular and thalamic surface morphometry in premature neonates, submitted to Neuroimage, 2012

[38] West J, Fitzpatrick JM, Wang MY, Dawant BM, Maurer CR Jr, Kessler RM, Maciunas RJ, Barillot C, Lemoine D, Collignon A, Maes F, Suetens P, Vandermeulen D, van den Elsen PA, Napel S, Sumanaweera TS, Harkness B, Hemler PF, Hill DL, Hawkes DJ, Studholme C, Maintz JB, Viergever MA, Malandain G, Woods RP, et al. Comparison and evaluation of retrospective intermodality brain image registration techniques. J Comput Assist Tomogr 21:554-566, 1997

[39] Yushkevich PA, Piven J, Hazlett HC, Smith RG, Ho S, Gee JC, Gerig G. User-guided 3D active contour segmentation of anatomical structures: Significantly improved efficiency and reliability. NeuroImage 31(3):1116-1128, 2006

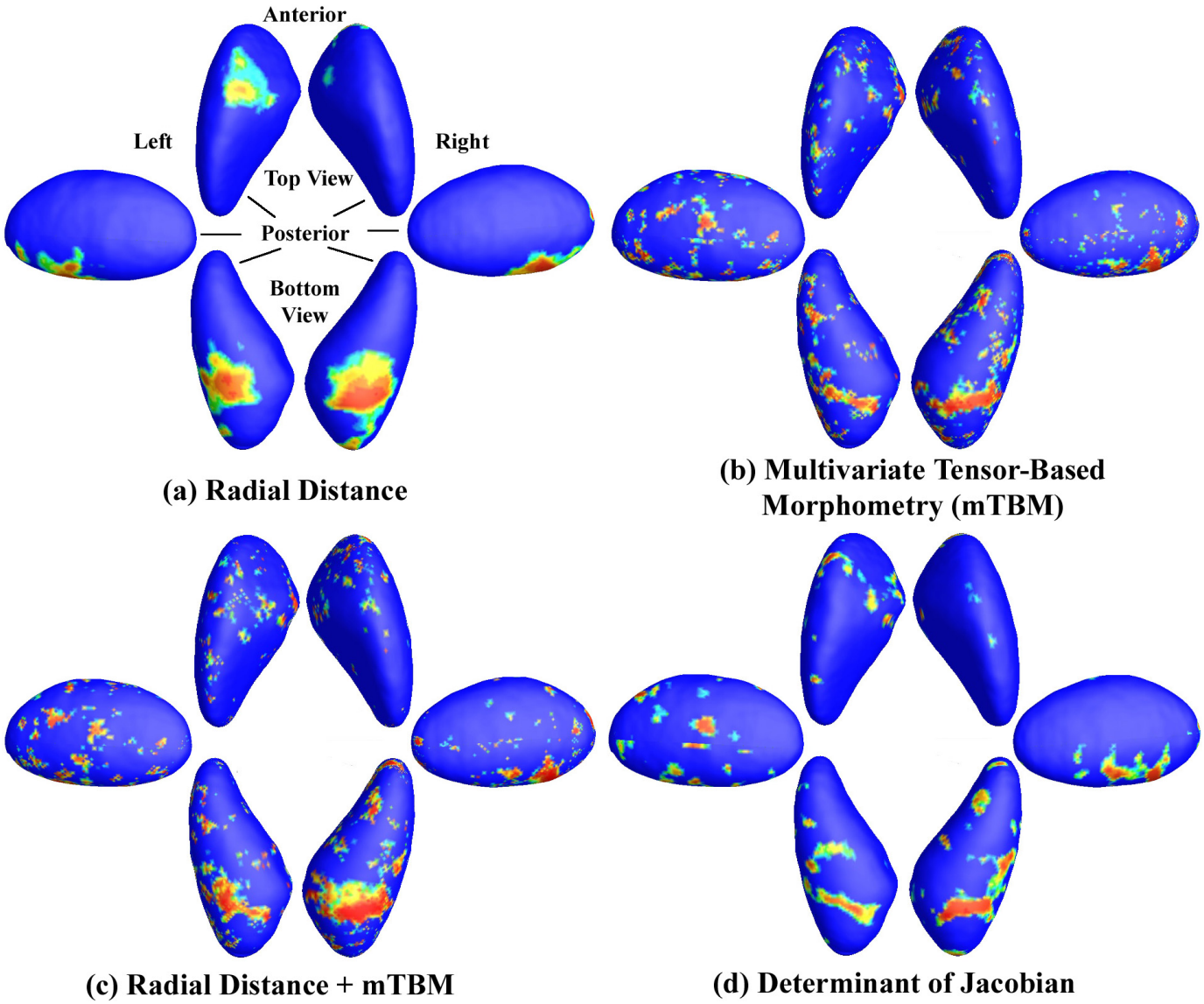

Fig. 2. Surface-based statistics. Top panel: P-values for the comparison of two groups, for 4 different statistics. The meaning of the different colors is shown in the colorbar. Whole map p-values were: (a) ρ: 0.0966; (b) S: 0.0206; (c) (ρ, S): 0.0177; (d) $detJ$:0.1021.

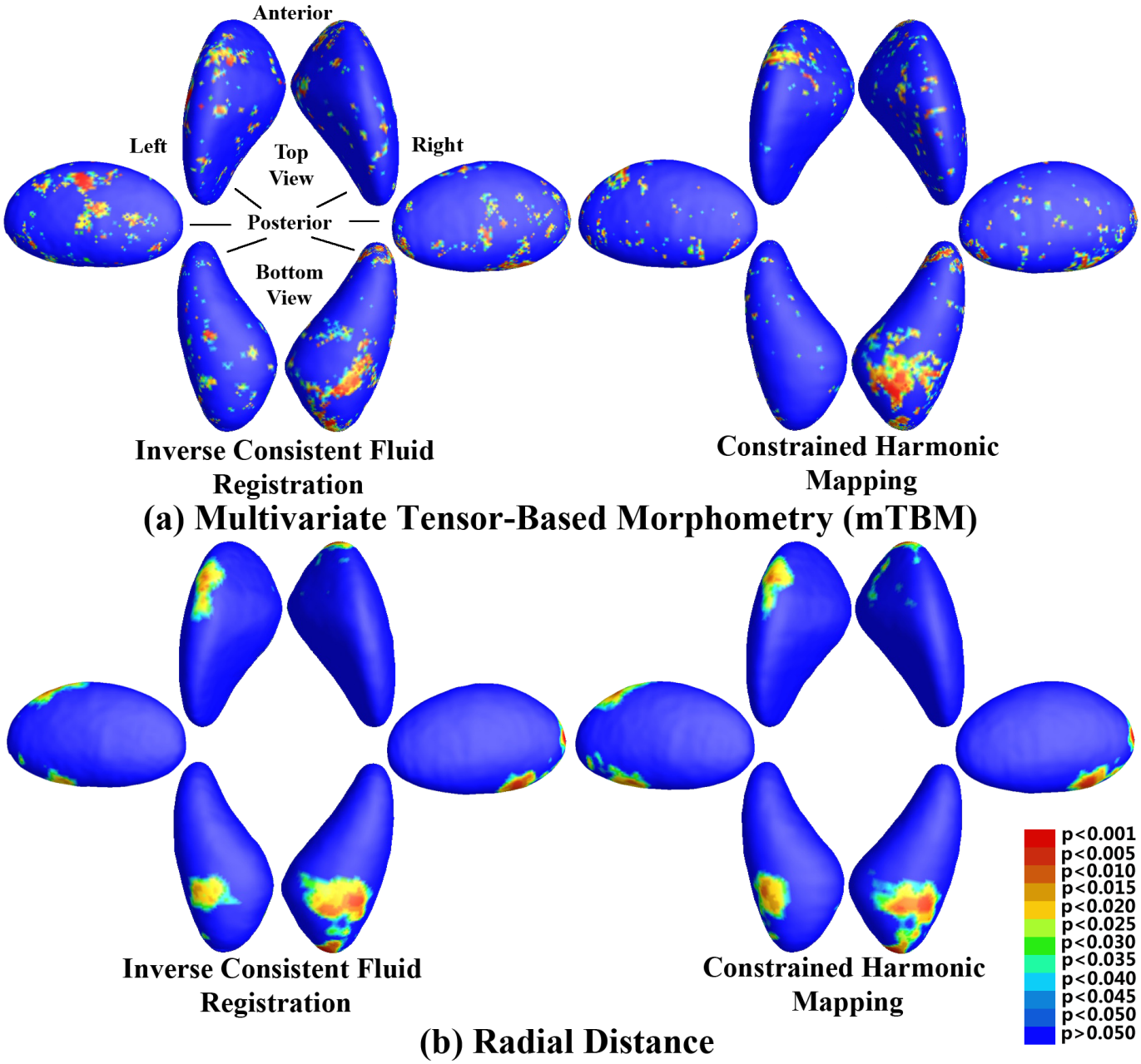

Fig. 3. Comparison of Fluid and constrained harmonic registrations **Top panel:** P-values for the comparison of S with the two registration methods. **Bottom panel**: P-values for the comparison of ρ with the two methods. The left column represents the fluid registration, while the right one is for the constrained harmonic mapping. The meaning of the different colors is shown in the colorbar. Whole map p-values for the constrained harmonic maps were: (a) ρ: 0.0889; (b) S: 0.055; (c) (ρ, S): 0.0362; (d) $detJ$: 0.0974.